Stoch Environ Res Risk Assess (2018) 32:905–919
https://doi.org/10.1007/s00477-017-1402-3

ORIGINAL PAPER

On a continuous spectral algorithm for simulating non-stationary Gaussian random fields

Xavier Emery[1,2] · **Daisy Arroyo**[1,2,3]

Published online: 24 March 2017

Abstract This paper presents an algorithm for simulating Gaussian random fields with zero mean and non-stationary covariance functions. The simulated field is obtained as a weighted sum of cosine waves with random frequencies and random phases, with weights that depend on the location-specific spectral density associated with the target non-stationary covariance. The applicability and accuracy of the algorithm are illustrated through synthetic examples, in which scalar and vector random fields with non-stationary Gaussian, exponential, Matérn or compactly-supported covariance models are simulated.

Keywords Turning bands · Fourier transform · Spectral density · Non-stationary covariance

1 Introduction

Geostatistical simulation is increasingly used in the earth and environmental sciences to characterize the uncertainty in the values of regionalized variables at locations where no measurement is available. Simulation relies on interpreting the regionalized variable as a realization of a parent random field, which can be characterized by its finite-dimensional distributions or, more synthetically, by its first-order moments (Chilès and Delfiner 2012).

Most of the time, an assumption of stationarity is made for inferring the model parameters (such as the expected value, the covariance or the univariate distribution) needed for simulation (Matheron 1971; Journel 1986). Stationarity states that the finite-dimensional distributions are invariant under a spatial translation and implies some form of spatial homogeneity of the random field under study. Although it is convenient, the use of stationary models may be questionable in some circumstances, as it may not allow accounting for local changes in the mean value (spatial trends), in the dispersion (proportional effects) or in the spatial continuity (e.g., local ranges of correlation, or local anisotropies explained by the presence of folded structures in geological formations such as petroleum reservoirs or ore deposits) of the regionalized variable under study.

For regionalized variables that exhibit a spatial trend, non-stationarity often concerns the first-order moment of the underlying random field, i.e., its expected value at each location, which can be modeled by expert knowledge or by fitting a trend model to the available data (Goovaerts 1997; Deutsch and Journel 1998; Costa 2009). In some occasions, the second-order moment (covariance function) is also assumed non-stationary, a situation that turns out to be more complex in relation with the definition of valid covariance models, with the inference of its parameters from a set of data and with the simulation of the random field. The first two problems (model definition and inference) are out of the scope of this paper. Varied theoretical and practical solutions have been proposed by Haas (1990), Monestiez and Switzer (1991), Sampson and Guttorp (1992), Guttorp and Sampson (1994), Smith (1996), Higdon et al. (1999), Damian et al. (2000), Sampson et al.

✉ Xavier Emery
xemery@ing.uchile.cl

Daisy Arroyo
darroyo@ing.uchile.cl

[1] Department of Mining Engineering, University of Chile, Santiago, Chile

[2] Advanced Mining Technology Center, University of Chile, Santiago, Chile

[3] Present Address: Department of Statistics, University of Concepción, Concepción, Chile

(2001), Higdon (2002), Nychka et al. (2002), Pintore and Holmes (2005), Stein (2005), Stephenson et al. (2005), Paciorek and Schervish (2006), Harris et al. (2010), Schlather (2010), Zhu and Wu (2010), Machuca-Mory and Deutsch (2013), Fouedjio et al. (2016) and Fouedjio and Séguret (2016), among others. Concerning the last problem (simulation), to date, several algorithms have been designed for constructing realizations of random fields with non-stationary covariances under an assumption that the finite-dimensional distributions are multivariate Gaussian: sequential simulation (Boisvert and Deutsch 2011), summation of Gaussian random fields with locally varying parameters (Fuentes 2002), dilution with locally varying kernel functions (Chilès and Delfiner 2012), moving averages and convolution approaches (Liang and Marcotte 2016), or Gibbs sampling (Fouedjio et al. 2016; Fouedjio and Séguret 2016).

In this context, this paper aims to present an alternative algorithm for simulating Gaussian random fields with non-stationary covariance functions, based on a decomposition of the field into cosine waves, and to illustrate the applicability of this algorithm through simple examples. Section 2 hereafter is devoted to the univariate case (scalar random fields), while the simulation of non-stationary vector random fields will be addressed in Sect. 3. A general discussion and conclusions follow in Sect. 4.

2 Univariate simulation

2.1 Spectral-turning bands simulation of a stationary random field

Consider a second-order stationary Gaussian random field defined in the d-dimensional Euclidean space, $Y = \{Y(\mathbf{x}): \mathbf{x} \in \mathbb{R}^d\}$, with zero mean, unit variance and covariance function $C(\mathbf{h})$, where $\mathbf{h}$ stands for a separation vector between two locations of $\mathbb{R}^d$. Provided that this covariance function is continuous and absolutely integrable, it can be written as the Fourier transform of a probability density function $f(\mathbf{u})$, with $\mathbf{u}$ defined on $\mathbb{R}^d$, called the spectral density of $C(\mathbf{h})$ (Bochner 1933):

$$\forall \mathbf{h} \in \mathbb{R}^d, C(\mathbf{h}) = \mathrm{F}\{f\}(\mathbf{h}) = \int_{\mathbb{R}^d} \cos(\langle \mathbf{u}|\mathbf{h}\rangle) f(\mathbf{u}) d\mathbf{u}, \quad (1)$$

where F indicates the Fourier transform and $\langle \mathbf{u}|\mathbf{h}\rangle = \mathbf{u}^T\mathbf{h}$ is the usual dot product in $\mathbb{R}^d$. This property of the covariance function allows simulating Y by a cosine wave of the form (Shinozuka 1971; Lantuéjoul 2002)

$$\forall \mathbf{x} \in \mathbb{R}^d, Y(\mathbf{x}) = \sqrt{2}\cos(\langle \mathbf{u}|\mathbf{x}\rangle + \phi), \quad (2)$$

where $\mathbf{u}$ is a random vector in $\mathbb{R}^d$ with probability density f and ϕ is an independent random variable uniformly distributed in $[0, 2\pi]$. Based on the central limit theorem, one can obtain a random field with approximately Gaussian finite-dimensional distributions by adding and rescaling many of such independent cosine waves (Lantuéjoul 2002):

$$\forall \mathbf{x} \in \mathbb{R}^d, Y(\mathbf{x}) = \sqrt{\frac{2}{L}} \sum_{l=1}^{L} \cos(\langle \mathbf{u}_l|\mathbf{x}\rangle + \phi_l), \quad (3)$$

where L is a large integer, $\{\mathbf{u}_l: l = 1, \ldots, L\}$ are mutually independent random vectors with probability density f, and $\{\phi_l: l = 1, \ldots, L\}$ are mutually independent random variables uniformly distributed in $[0, 2\pi]$, independent of $\{\mathbf{u}_l: l = 1, \ldots, L\}$.

This method appears as a particular case of the turning bands algorithm (Matheron 1973) and allows simulating stationary Gaussian random fields based on the spectral density of their covariance functions. Shinozuka (1971) and Shinozuka and Jan (1972) proposed a variant of this method, by simulating the random vectors $\{\mathbf{u}_l: l = 1, \ldots, L\}$ according to a uniform distribution instead of the spectral distribution, then adequately weighting the cosine waves. However, this approach is approximate unless the spectral density f has a bounded support. Emery et al. (2016) propose replacing the uniform distribution by another one, say g, with a support containing that of f, in the following fashion:

$$\forall \mathbf{x} \in \mathbb{R}^d, Y(\mathbf{x}) = \frac{1}{\sqrt{L}} \sum_{l=1}^{L} \sqrt{\frac{2f(\mathbf{u}_l)}{g(\mathbf{u}_l)}} \cos(\langle \mathbf{u}_l|\mathbf{x}\rangle + \phi_l), \quad (4)$$

where $\{\mathbf{u}_l: l = 1, \ldots, L\}$ are mutually independent random vectors with probability density g and $\{\phi_l: l = 1, \ldots, L\}$ are mutually independent random variables uniformly distributed in $[0, 2\pi]$, independent of $\{\mathbf{u}_l: l = 1, \ldots, L\}$. It can be shown that the random field Y so defined is second-order stationary, with zero mean and covariance function $C(\mathbf{h})$ and, if L is large, its finite-dimensional distributions are nearly Gaussian (Emery et al. 2016).

Unlike Eq. (3), Eq. (4) dissociates the choice of the distribution of the frequency vectors $\{\mathbf{u}_l: l = 1, \ldots, L\}$ (density g) from the choice of the covariance function of the target random field (density f), which amounts to an importance sampling strategy. This strategy allows generalizing the spectral algorithm to the simulation of random fields with stationary increments or generalized increments (Emery and Lantuéjoul 2008; Arroyo and Emery 2017). In the following subsection, we will adapt it to the simulation of random fields with non-stationary covariance functions.

2.2 A proposal for simulating a non-stationary random field

Let us now define a random field Y in the d-dimensional Euclidean space as follows:

$$\forall \mathbf{x} \in \mathbb{R}^d, Y(\mathbf{x}) = \sqrt{\frac{2f_{\mathbf{x}}(\mathbf{u})}{g(\mathbf{u})}}\cos(\langle \mathbf{u}|\mathbf{x}\rangle + \phi), \tag{5}$$

where $\mathbf{u}$ is a random vector with density g, ϕ is an independent uniform random variable in $[0, 2\pi]$ and $f_{\mathbf{x}}$ now depends on the target location $\mathbf{x}$. Because ϕ is uniform, the mean value of Y is zero. The covariance between two variables $Y(\mathbf{x})$ and $Y(\mathbf{x}')$ is

$$\begin{aligned} C(\mathbf{x},\mathbf{x}') &:= \mathrm{cov}\{Y(\mathbf{x}), Y(\mathbf{x}')\} \\ &= E\left\{\frac{2\sqrt{f_{\mathbf{x}}(\mathbf{u})f_{\mathbf{x}'}(\mathbf{u})}}{g(\mathbf{u})}\cos(\langle \mathbf{u}|\mathbf{x}\rangle + \phi)\cos(\langle \mathbf{u}|\mathbf{x}'\rangle + \phi)\right\} \\ &= E\left\{\frac{\sqrt{f_{\mathbf{x}}(\mathbf{u})f_{\mathbf{x}'}(\mathbf{u})}}{g(\mathbf{u})}\cos(\langle \mathbf{u}|\mathbf{x}-\mathbf{x}'\rangle)\right\} \\ &= \int_{\mathbb{R}^d} \cos(\langle \mathbf{u}|\mathbf{x}-\mathbf{x}'\rangle)\sqrt{f_{\mathbf{x}}(\mathbf{u})f_{\mathbf{x}'}(\mathbf{u})}d\mathbf{u}. \end{aligned} \tag{6}$$

This is the Fourier transform of the geometric average of the spectral densities associated with locations $\mathbf{x}$ and $\mathbf{x}'$:

$$C(\mathbf{x},\mathbf{x}') = \mathrm{F}\left\{\sqrt{f_{\mathbf{x}}f_{\mathbf{x}'}}\right\}(\mathbf{x}-\mathbf{x}'). \tag{7}$$

If one denotes by $\varpi_{\mathbf{x}}$ the Fourier transform of $\sqrt{f_{\mathbf{x}}}$, one also has:

$$C(\mathbf{x},\mathbf{x}') = (\varpi_{\mathbf{x}} * \varpi_{\mathbf{x}'})(\mathbf{x}-\mathbf{x}'), \tag{8}$$

where * stands for the convolution product.

By virtue of the central limit theorem, to obtain a random field whose finite-dimensional distributions are approximately multivariate-Gaussian, it is necessary to add numerous independent components as in Eq. (4):

$$\forall \mathbf{x} \in \mathbb{R}^d, Y(\mathbf{x}) = \frac{1}{\sqrt{L}}\sum_{l=1}^{L}\sqrt{\frac{2f_{\mathbf{x}}(\mathbf{u}_l)}{g(\mathbf{u}_l)}}\cos(\langle \mathbf{u}_l|\mathbf{x}\rangle + \phi_l), \tag{9}$$

where L is a large integer, $\{\mathbf{u}_l: l = 1, \ldots, L\}$ are mutually independent random vectors with probability density g, and $\{\phi_l: l = 1, \ldots, L\}$ are mutually independent random variables uniformly distributed in $[0, 2\pi]$, independent of $\{\mathbf{u}_l: l = 1, \ldots, L\}$. This is but a special case of the turning bands method, where the random vectors $\{\mathbf{u}_l: l = 1, \ldots, L\}$ define a set of lines that span $\mathbb{R}^d$ and a cosine wave is simulated along each line.

2.3 Examples

2.3.1 Geometric anisotropy modeling

In this section, we are interested in simulating random fields whose covariance functions have a geometric anisotropy with locally varying scale factors and/or anisotropy directions. A stationary covariance function $C(\mathbf{h})$ with a geometric anisotropy is obtained by combining a stationary isotropic covariance function $C_0(\mathbf{h})$ and a $d \times d$ symmetric positive semi-definite matrix Σ (Journel and Huijbregts 1978; Chilès and Delfiner 2012):

$$\forall \mathbf{h} \in \mathbb{R}^d, C(\mathbf{h}) = C_0(\Sigma^{-1/2}\mathbf{h}). \tag{10}$$

In the following, Σ will be referred to as the anisotropy matrix. Let f_0 be the spectral density of C_0. Then

$$\begin{aligned} C(\mathbf{h}) &= C_0(\Sigma^{-1/2}\mathbf{h}) \\ &= \int_{\mathbb{R}^d} \cos\left(\left\langle \mathbf{u}|\Sigma^{-1/2}\mathbf{h}\right\rangle\right) f_0(\mathbf{u})d\mathbf{u} \\ &= \int_{\mathbb{R}^d} \cos\left(\left\langle \Sigma^{-1/2}\mathbf{u}|\mathbf{h}\right\rangle\right) f_0(\mathbf{u})d\mathbf{u} \\ &= |\Sigma|^{1/2}\int_{\mathbb{R}^d} \cos(\langle \mathbf{v}|\mathbf{h}\rangle) f_0(\Sigma^{1/2}\mathbf{v})d\mathbf{v}, \end{aligned} \tag{11}$$

where $|\Sigma|$ stands for the determinant of Σ. Accordingly, the spectral density of C is

$$f(\mathbf{u}) = |\Sigma|^{1/2} f_0(\Sigma^{1/2}\mathbf{u}). \tag{12}$$

This result agrees with the one presented by Marcotte (2015).

2.3.2 Non-stationary Gaussian covariance

Consider a stationary isotropic Gaussian covariance function with unit variance and unit scale factor

$$\forall \mathbf{h} \in \mathbb{R}^d, C_0^G(\mathbf{h}) = \exp(-\mathbf{h}^T\mathbf{h}). \tag{13}$$

The spectral density of C_0^G is (Lantuéjoul 2002):

$$f_0^G(\mathbf{u}) = \frac{1}{(2\sqrt{\pi})^d}\exp\left\{-\frac{1}{4}\mathbf{u}^T\mathbf{u}\right\}. \tag{14}$$

Let us now simulate a non-stationary random field as in Eq. (9), by considering the spectral density $f_{\Sigma_{\mathbf{x}}}^G$ of a Gaussian covariance associated with an anisotropy matrix $\Sigma_{\mathbf{x}}$ that depends on $\mathbf{x}$. Because of Eqs. (7) and (12), the covariance of the simulated field at two given locations $\mathbf{x}$ and $\mathbf{x}'$ is

$$C^G(\mathbf{x},\mathbf{x}',\Sigma_{\mathbf{x}},\Sigma_{\mathbf{x}'}) = \mathrm{F}\left\{\sqrt{f_{\Sigma_{\mathbf{x}}}^G f_{\Sigma_{\mathbf{x}'}}^G}\right\}(\mathbf{x}-\mathbf{x}'), \tag{15}$$

with

$$\begin{aligned} \sqrt{f_{\Sigma_{\mathbf{x}}}^G(\mathbf{u})f_{\Sigma_{\mathbf{x}'}}^G(\mathbf{u})} &= \sqrt{|\Sigma_{\mathbf{x}}|^{1/2}|\Sigma_{\mathbf{x}'}|^{1/2} f_0^G\left(\Sigma_{\mathbf{x}}^{1/2}\mathbf{u}\right) f_0^G\left(\Sigma_{\mathbf{x}'}^{1/2}\mathbf{u}\right)} \\ &= |\Sigma_{\mathbf{x}}|^{1/4}|\Sigma_{\mathbf{x}'}|^{1/4}\frac{1}{(2\sqrt{\pi})^d} \\ &\quad \times \exp\left\{-\frac{1}{4}\mathbf{u}^T\left(\frac{\Sigma_{\mathbf{x}}+\Sigma_{\mathbf{x}'}}{2}\right)\mathbf{u}\right\} \\ &= |\Sigma_{\mathbf{x}}|^{1/4}|\Sigma_{\mathbf{x}'}|^{1/4} f_0^G\left(\left(\frac{\Sigma_{\mathbf{x}}+\Sigma_{\mathbf{x}'}}{2}\right)^{1/2}\mathbf{u}\right) \\ &= |\Sigma_{\mathbf{x}}|^{1/4}|\Sigma_{\mathbf{x}'}|^{1/4}\left|\frac{\Sigma_{\mathbf{x}}+\Sigma_{\mathbf{x}'}}{2}\right|^{-1/2} f_{(\Sigma_{\mathbf{x}}+\Sigma_{\mathbf{x}'})/2}^G(\mathbf{u}), \end{aligned} \tag{16}$$

where $f^G_{(\Sigma_{\mathbf{x}}+\Sigma_{\mathbf{x}'})/2}$ is the spectral density of the Gaussian covariance with anisotropy matrix $\frac{\Sigma_{\mathbf{x}}+\Sigma_{\mathbf{x}'}}{2}$ (Eq. 12). Accordingly, the non-stationary covariance of the simulated field is proportional to this anisotropic Gaussian covariance:

$$C^G(\mathbf{x},\mathbf{x}',\Sigma_{\mathbf{x}},\Sigma_{\mathbf{x}'}) = |\Sigma_{\mathbf{x}}|^{1/4}|\Sigma_{\mathbf{x}'}|^{1/4}\left|\frac{\Sigma_{\mathbf{x}}+\Sigma_{\mathbf{x}'}}{2}\right|^{-1/2} \times \exp\left\{-(\mathbf{x}-\mathbf{x}')^T\left(\frac{\Sigma_{\mathbf{x}}+\Sigma_{\mathbf{x}'}}{2}\right)^{-1}(\mathbf{x}-\mathbf{x}')\right\}. \quad (17)$$

This non-stationary Gaussian covariance model has already been introduced by Paciorek and Schervish (2006). The proposed spectral algorithm (Eq. 9) therefore provides a simple way to simulate a Gaussian random field with such a covariance.

As an example, consider a regular grid with 201 × 201 nodes and unit internode distance in the two-dimensional space, and an anisotropy matrix depending on the y-coordinate only, such that the practical range in all directions is equal to 5 for $y = 0$ and to 30 for $y = 200$ (recall that the practical range of a Gaussian covariance is defined as $\sqrt{3}$ times its scale factor). Figure 1a displays a map of one realization obtained with the proposed spectral algorithm (Eq. 9) using $L = 5000$ lines and taking g as the spectral density of an isotropic Matérn covariance with scale factor 3 and shape parameter 0.3 (Lantuéjoul 2002). Figure 1b plots the experimental cumulative distribution functions of one hundred realizations, together with the theoretical standard Gaussian cumulative distribution function. It is seen that the former fluctuate around the latter, with an almost perfect match on average over the realizations. Figure 1c (resp. Fig. 1d) plots the experimental variograms of one hundred realizations, calculated between the grid nodes with coordinates $(x, 100)$ and $(x, 100 - h)$ (resp. $(x, 200)$ and $(x, 200 - h)$), where x goes from 0 to 200, for lag separation distances h varying between 0 and 30, together with the theoretical variogram derived from Eq. (17) for the same pairs of coordinates. On average over all the realizations, the match between experimental and theoretical variograms is almost perfect, which corroborates the correctness of the proposed simulation algorithm. As expected, the fluctuations of the experimental variograms around the theoretical model are small at small lag distances and become larger and larger when this distance increases (Matheron 1971, 1989; Chilès and Delfiner 2012). The spread of these statistical fluctuations may call the attention to readers who are familiar with the simulation of stationary Gaussian random fields on a so large grid in relation to the practical range of correlation. This is explained because, in the stationary case, the experimental variogram at a given lag separation distance h would be calculated on the basis of 201 × (201 − h) pairs of grid nodes, whereas in the present case we are calculating local variograms on the basis of only 201 pairs of grid nodes, which irremediably yields greater fluctuations.

2.3.3 Non-stationary exponential covariance

Consider now a stationary isotropic exponential covariance function with unit variance and unit scale factor:

$$C_0^E(\mathbf{h}) = \exp(-\sqrt{\mathbf{h}^T\mathbf{h}}). \quad (18)$$

The spectral density of C_0^E is (Lantuéjoul 2002):

$$f_0^E(\mathbf{u}) = \frac{\Gamma\left(\frac{d+1}{2}\right)}{\pi^{(d+1)/2}}\frac{1}{(1+\mathbf{u}^T\mathbf{u})^{(d+1)/2}}. \quad (19)$$

If one considers the spectral density $f^E_{\Sigma_{\mathbf{x}}}$ of an exponential covariance with an anisotropy matrix $\Sigma_{\mathbf{x}}$ that depends on $\mathbf{x}$ (Eq. 12) and plug it into Eq. (7), the resulting covariance function is no longer an exponential function. To avoid this inconvenience, an alternative is to view the exponential covariance as a scale mixture of Gaussian covariances, where the scale factor is twice the square root of a standard gamma random variable with shape parameter 0.5 (Emery and Lantuéjoul 2006):

$$C_0^E(\mathbf{h}) = \frac{1}{\Gamma(1/2)}\int_0^{+\infty} C_0^G\left(\frac{\mathbf{h}}{2\sqrt{a}}\right)a^{-1/2}\exp(-a)da. \quad (20)$$

The simulation can therefore be performed by using, in Eq. (9), a Gaussian spectral density associated with an anisotropy matrix that depends not only on the target location $\mathbf{x}$, but also on the line index l. Specifically, for $l \in \{1, \ldots, L\}$, one should simulate a standard gamma random variable a_l with shape parameter 0.5, then rescale the anisotropy matrix at any location $\mathbf{x}$, $\Sigma_{\mathbf{x}}$, by four times the scale factor a_l, i.e., use the local density

$$f^G_{4a_l\Sigma_{\mathbf{x}}}(\mathbf{u}) = |4a_l\Sigma_{\mathbf{x}}|^{1/2}f_0^G\left\{(4a_l\Sigma_{\mathbf{x}})^{1/2}\mathbf{u}\right\}. \quad (21)$$

For a given realization of a_l, the cosine wave simulated along the line with index l has therefore the following Gaussian covariance (Eq. 17):

$$C^G(\mathbf{x},\mathbf{x}',4a_l\Sigma_{\mathbf{x}},4a_l\Sigma_{\mathbf{x}'}) = |\Sigma_{\mathbf{x}}|^{1/4}|\Sigma_{\mathbf{x}'}|^{1/4}\left|\frac{\Sigma_{\mathbf{x}}+\Sigma_{\mathbf{x}'}}{2}\right|^{-1/2} \times C_0^G\left(\left(4a_l\frac{\Sigma_{\mathbf{x}}+\Sigma_{\mathbf{x}'}}{2}\right)^{-1/2}(\mathbf{x}-\mathbf{x}')\right). \quad (22)$$

Based on Eq. (20), the prior covariance (when averaging over all the possible values of a_l weighted by their respective densities) is found to be:

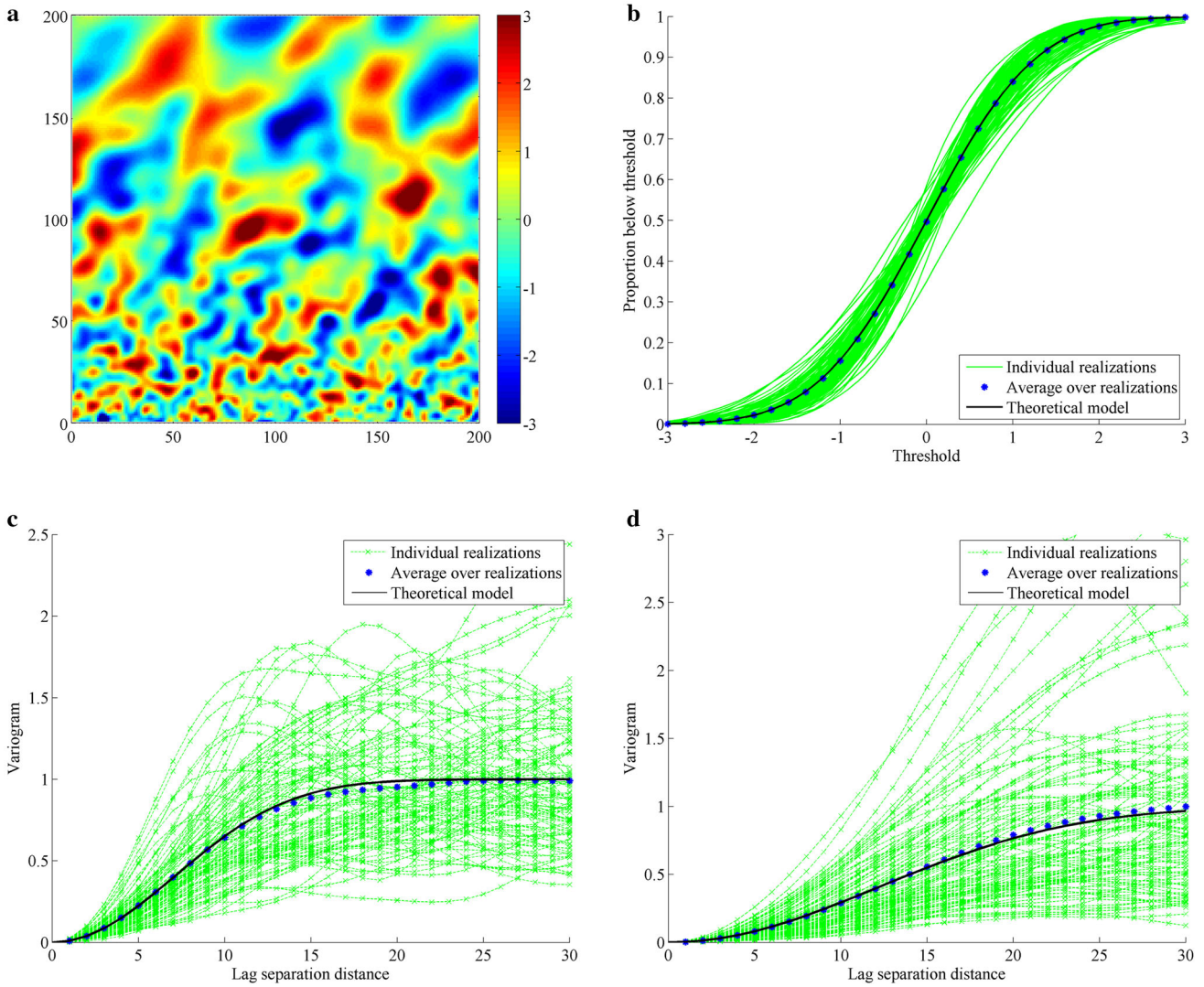

Fig. 1 **a** Realization of a random field with non-stationary Gaussian covariance with varying practical range, **b** cumulative distribution functions of 100 realizations, and **c**, **d** local variograms of 100 realizations

$$
\begin{aligned}
&C^E(\mathbf{x},\mathbf{x}',\boldsymbol{\Sigma}_{\mathbf{x}},\boldsymbol{\Sigma}_{\mathbf{x}'})\\
&\quad=\frac{1}{\Gamma(1/2)}\int_0^{+\infty} C^G(\mathbf{x},\mathbf{x}',4a\boldsymbol{\Sigma}_{\mathbf{x}},4a\boldsymbol{\Sigma}_{\mathbf{x}'})a^{-1/2}\exp(-a)da\\
&\quad=\frac{|\boldsymbol{\Sigma}_{\mathbf{x}}|^{1/4}|\boldsymbol{\Sigma}_{\mathbf{x}'}|^{1/4}}{\Gamma(1/2)}\left|\frac{\boldsymbol{\Sigma}_{\mathbf{x}}+\boldsymbol{\Sigma}_{\mathbf{x}'}}{2}\right|^{-1/2}\\
&\qquad\times\int_0^{+\infty} C_0^G\left(\left(4a\frac{\boldsymbol{\Sigma}_{\mathbf{x}}+\boldsymbol{\Sigma}_{\mathbf{x}'}}{2}\right)^{-1/2}(\mathbf{x}-\mathbf{x}')\right)a^{-1/2}\exp(-a)da\\
&\quad=|\boldsymbol{\Sigma}_{\mathbf{x}}|^{1/4}|\boldsymbol{\Sigma}_{\mathbf{x}'}|^{1/4}\left|\frac{\boldsymbol{\Sigma}_{\mathbf{x}}+\boldsymbol{\Sigma}_{\mathbf{x}'}}{2}\right|^{-1/2}C_0^E\left(\left(\frac{\boldsymbol{\Sigma}_{\mathbf{x}}+\boldsymbol{\Sigma}_{\mathbf{x}'}}{2}\right)^{-1/2}(\mathbf{x}-\mathbf{x}')\right).
\end{aligned}
\tag{23}
$$

Equivalently:

$$
\begin{aligned}
C^E(\mathbf{x},\mathbf{x}',\boldsymbol{\Sigma}_{\mathbf{x}},\boldsymbol{\Sigma}_{\mathbf{x}'}) &= |\boldsymbol{\Sigma}_{\mathbf{x}}|^{1/4}|\boldsymbol{\Sigma}_{\mathbf{x}'}|^{1/4}\left|\frac{\boldsymbol{\Sigma}_{\mathbf{x}}+\boldsymbol{\Sigma}_{\mathbf{x}'}}{2}\right|^{-1/2}\\
&\times\exp\left\{-\sqrt{(\mathbf{x}-\mathbf{x}')^T\left(\frac{\boldsymbol{\Sigma}_{\mathbf{x}}+\boldsymbol{\Sigma}_{\mathbf{x}'}}{2}\right)^{-1}(\mathbf{x}-\mathbf{x}')}\right\},
\end{aligned}
\tag{24}
$$

which coincides with the non-stationary exponential covariance introduced by Paciorek and Schervish (2006).

An experiment similar to that of Fig. 1 is presented in Fig. 2, where here the simulated field has an isotropic exponential covariance with a practical range equal to 5 for $y = 0$ and to 30 for $y = 200$ (the practical range of an exponential covariance is defined as 3 times its scale factor). The realization on the 201×201 grid mapped in Fig. 2a is obtained by using $L = 5000$ lines and the spectral density of an isotropic Matérn covariance with scale factor 3 and shape parameter 0.3 for g. The experimental cumulative distribution functions of one hundred realizations are plotted in Fig. 2b, while Fig. 2c (resp. Fig. 2d) displays their experimental variograms calculated between the grid nodes with coordinates $(x,\ 100)$ and $(x,\ 100 - h)$ [resp. $(x,\ 200)$ and $(x,\ 200 - h)$], where x goes

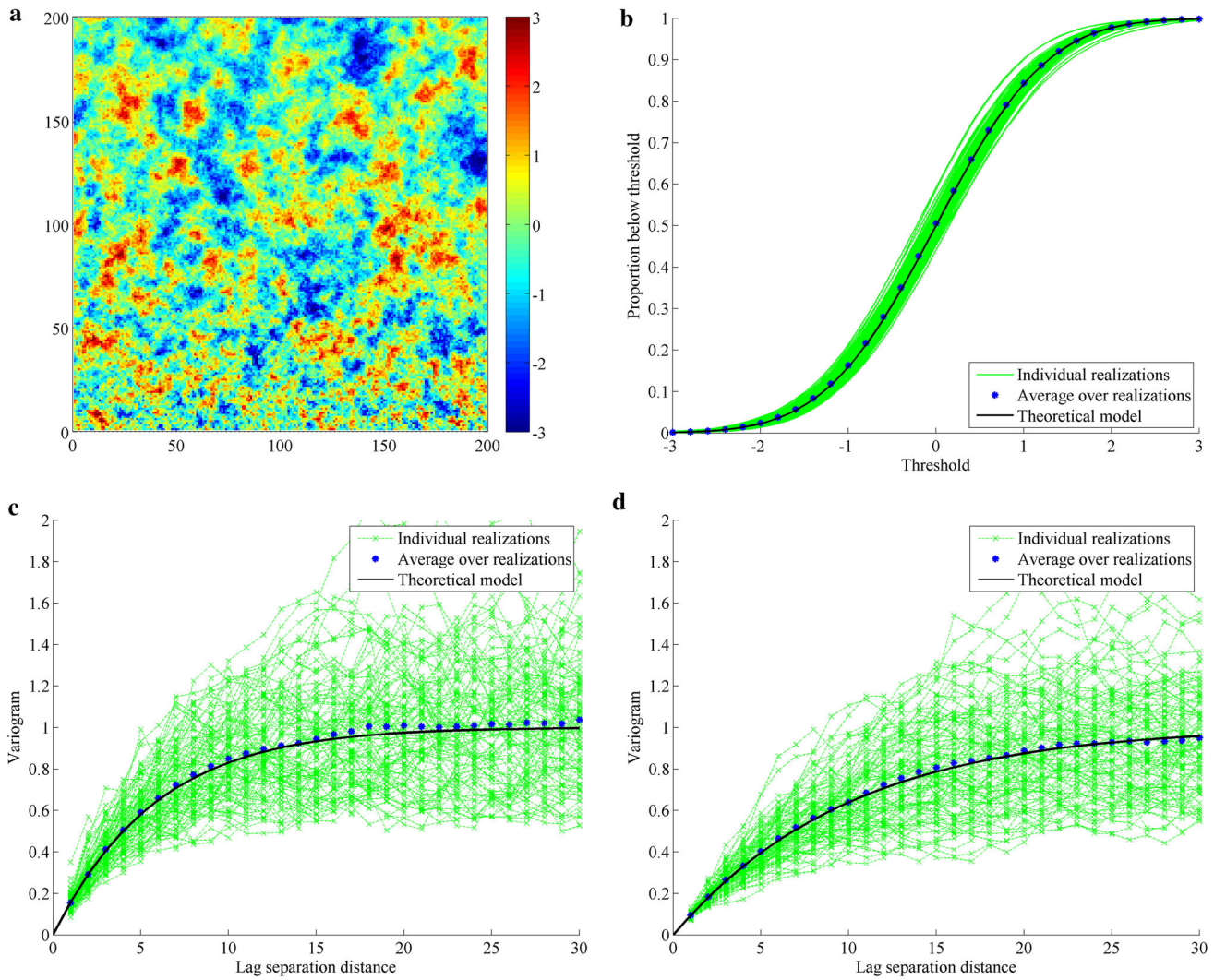

Fig. 2 **a** Realization of a random field with non-stationary exponential covariance with varying practical range, **b** cumulative distribution functions of 100 realizations, and **c**, **d** local variograms of 100 realizations

from 0 to 200, for lag separation distances h varying from 0 to 30. It is observed that, on average over all the realizations, the experimental distributions and the experimental variograms match their respective theoretical models. Interestingly, the spreads of their statistical fluctuations are smaller than the ones observed in the experiment made with the Gaussian covariance (Sect. 2.3.2). Such a difference can be explained because of the smoothness of the random fields with a Gaussian covariance (as opposed to random fields with an exponential covariance), an effect already discussed by Matheron (1971) and Chilès and Delfiner (2012).

2.3.4 Non-stationary Matérn covariance

In the previous subsection, if one uses a standard gamma random variable a_l with shape parameter $\mu > 0$ instead of 0.5, one obtains a Matérn covariance with shape parameter μ, as a scale mixture of Gaussian covariances (Emery and Lantuéjoul 2006):

$$\begin{aligned} &C^M(\mathbf{x},\mathbf{x}',\boldsymbol{\Sigma}_{\mathbf{x}},\boldsymbol{\Sigma}_{\mathbf{x}'},\mu) \\ &= \frac{|\boldsymbol{\Sigma}_{\mathbf{x}}|^{1/4}|\boldsymbol{\Sigma}_{\mathbf{x}'}|^{1/4}}{\Gamma(\mu)}\left|\frac{\boldsymbol{\Sigma}_{\mathbf{x}}+\boldsymbol{\Sigma}_{\mathbf{x}'}}{2}\right|^{-1/2} \\ &\quad\times\int_0^{+\infty} C_0^G\left(\left(4a\frac{\boldsymbol{\Sigma}_{\mathbf{x}}+\boldsymbol{\Sigma}_{\mathbf{x}'}}{2}\right)^{-1/2}(\mathbf{x}-\mathbf{x}')\right)a^{\mu-1}\exp(-a)da \\ &= |\boldsymbol{\Sigma}_{\mathbf{x}}|^{1/4}|\boldsymbol{\Sigma}_{\mathbf{x}'}|^{1/4}\left|\frac{\boldsymbol{\Sigma}_{\mathbf{x}}+\boldsymbol{\Sigma}_{\mathbf{x}'}}{2}\right|^{-1/2} C^M\left(\mathbf{x}-\mathbf{x}',\frac{\boldsymbol{\Sigma}_{\mathbf{x}}+\boldsymbol{\Sigma}_{\mathbf{x}'}}{2},\mu\right), \end{aligned} \tag{25}$$

where $C^M(\mathbf{h},\boldsymbol{\Sigma},\mu) = \frac{1}{2^{\mu-1}\Gamma(\mu)}(\sqrt{\mathbf{h}^T\boldsymbol{\Sigma}^{-1}\mathbf{h}})^{\mu}K_{\mu}(\sqrt{\mathbf{h}^T\boldsymbol{\Sigma}^{-1}\mathbf{h}})$ is the stationary Matérn covariance with anisotropy matrix $\boldsymbol{\Sigma}$ and shape parameter μ, and K_{μ} is the modified Bessel function of the second kind of order μ.

However, this construction does not allow the shape parameter μ to vary in space. To overcome this limitation, let us consider the use, for the line with index $l \in \{1, \ldots, L\}$, of a scale factor a_l drawn from a standard gamma distribution with shape parameter 1 (i.e., a_l is a realization of an exponential variable) and a spectral density of the following form:

$$f^M_{\Sigma_{\mathbf{x}},\mu(\mathbf{x}),a_l}(\mathbf{u}) = \frac{a_l^{\mu(\mathbf{x})-1}}{\Gamma(\mu(\mathbf{x}))} f^G_{4a_l\Sigma_{\mathbf{x}}}(\mathbf{u}) = \frac{a_l^{\mu(\mathbf{x})-1}}{\Gamma(\mu(\mathbf{x}))} |4a_l\Sigma_{\mathbf{x}}|^{1/2} f_0^G\left\{(4a_l\Sigma_{\mathbf{x}})^{1/2}\mathbf{u}\right\}, \quad (26)$$

where $\mu(\mathbf{x})$ is a positive scalar that depends on location $\mathbf{x}$. The covariance between the variables simulated at two locations $\mathbf{x}$ and $\mathbf{x}'$ (Eq. 25) becomes:

$$\begin{aligned} &C^M(\mathbf{x},\mathbf{x}',\Sigma_{\mathbf{x}},\Sigma_{\mathbf{x}'},\mu(\mathbf{x}),\mu(\mathbf{x}')) \\ &= \frac{|\Sigma_{\mathbf{x}}|^{1/4}|\Sigma_{\mathbf{x}'}|^{1/4}}{\sqrt{\Gamma(\mu(\mathbf{x}))\Gamma(\mu(\mathbf{x}'))}} \left|\frac{\Sigma_{\mathbf{x}}+\Sigma_{\mathbf{x}'}}{2}\right|^{-1/2} \\ &\quad \times \int_0^{+\infty} a^{\frac{\mu(\mathbf{x})+\mu(\mathbf{x}')}{2}-1} C_0^G\left(\left(4a\frac{\Sigma_{\mathbf{x}}+\Sigma_{\mathbf{x}'}}{2}\right)^{-1/2}(\mathbf{x}-\mathbf{x}')\right)\exp(-a)da \\ &= \frac{1}{\sqrt{\Gamma(\mu(\mathbf{x}))\Gamma(\mu(\mathbf{x}'))}}\Gamma\left(\frac{\mu(\mathbf{x})+\mu(\mathbf{x}')}{2}\right) \\ &\quad \times C^M\left(\mathbf{x},\mathbf{x}',\Sigma_{\mathbf{x}},\Sigma_{\mathbf{x}'},\frac{\mu(\mathbf{x})+\mu(\mathbf{x}')}{2}\right). \end{aligned} \quad (27)$$

This is a Matérn covariance, with unit variance ($C^M(\mathbf{x},\mathbf{x},\Sigma_{\mathbf{x}},\Sigma_{\mathbf{x}},\mu(\mathbf{x}),\mu(\mathbf{x})) = 1$ for any $\mathbf{x}$), anisotropy matrix $\frac{\Sigma_{\mathbf{x}}+\Sigma_{\mathbf{x}'}}{2}$ and shape parameter $\frac{\mu(\mathbf{x})+\mu(\mathbf{x}')}{2}$.

As an illustration, consider the previous regular 2D grid with 201 × 201 nodes and define an isotropic Matérn covariance with constant scale factor 10 and varying shape parameter $\mu(\mathbf{x}) = \mu(x, y)$ that varies linearly with the ordinate y, such that $\mu(x, 0) = 0.5$ and $\mu(x, 200) = 1.5$. As previously, the spectral simulation is performed with $L = 5000$ lines and with the spectral density of an isotropic Matérn covariance with scale factor 3 and shape parameter 0.3 for g. One realization is mapped in Fig. 3a, where one observes smoother spatial variations in the top of the map (explained because of the higher shape parameter) and rougher spatial variations in the bottom part (because of the lower shape parameter). The experimental cumulative distribution functions of one hundred realizations are displayed in Fig. 3b, while their experimental variograms, calculated between the grid nodes with coordinates $(x, 100)$ and $(x, 100 - h)$ [resp. $(x, 200)$ and $(x, 200 - h)$], where x goes from 0 to 200, for lag separation distances h varying between 0 and 30, are displayed in Fig. 3c (resp. Fig. 3d). Again, no bias is perceptible in the reproduction of the distribution and of the spatial correlation structure, since the average of the experimental cumulative distribution functions and the average of the experimental variograms coincide with their respective theoretical models.

One can easily simulate Gaussian random fields with more complex non-stationary Matérn covariance functions, for which not only the shape parameter, but also the scale factors and anisotropy directions (codified into the anisotropy matrix $\Sigma_{\mathbf{x}}$) vary in space. For instance, consider an anisotropic Matérn covariance with the largest (respectively, the smallest) scale factor that linearly varies from 3 (respectively, 1) for $x = 0$ to 9 (respectively, 3) for $x = 200$, so that the anisotropy ratio remains equal to 3 everywhere, a shape parameter that linearly varies from 0.5 for $y = 0$ to 1.5 for $y = 200$, and a local azimuth for the direction with the largest scale factor as shown in Fig. 4b. One realization of a Gaussian random field with such a non-stationary Matérn covariance is mapped in Fig. 4a, where the spatial variations combine a progressive increase of the scale factor when moving from left to right, a progressive decrease of the smoothness when moving from top to bottom, and a vortex-type anisotropy.

2.3.5 Non-stationary compactly supported covariance

All the previous covariance models (Gaussian, exponential and Matérn) have an unbounded support, i.e. they vanish asymptotically with the lag separation distance but remain different from zero everywhere. To obtain a compactly supported covariance model, a simple option is to consider the spectral density of, say, an isotropic spherical covariance C_a^S with range a in the 3D space (Lantuéjoul 2002):

$$f_a^S(\mathbf{u}) = \frac{3a^3}{4\pi(\mathbf{u}^T\mathbf{u})^{3/2}} J_{3/2}^2\left(a\frac{\sqrt{\mathbf{u}^T\mathbf{u}}}{2}\right). \quad (28)$$

Up to a normalization factor, the spherical covariance with range a is the auto-convolution of the indicator of a 3D ball with diameter a:

$$C_a^S(\mathbf{h}) = (\varpi_a * \varpi_a)(\mathbf{h}), \quad (29)$$

where ϖ_a is the Fourier transform of $\sqrt{f_a^S}$ (Eq. 8). If the range, now denoted as $a(\mathbf{x})$, varies in space, then one obtains a non-stationary covariance of the form

$$C^S(\mathbf{x},\mathbf{x}',a(\mathbf{x}),a(\mathbf{x}')) = (\varpi_{a(\mathbf{x})} * \varpi_{a(\mathbf{x}')})(\mathbf{x}-\mathbf{x}'), \quad (30)$$

which coincides with the volume of the intersection of two balls, with respective diameters $a(\mathbf{x})$ and $a(\mathbf{x}')$, centered at $\mathbf{x}$ and $\mathbf{x}'$, rescaled in such a way that $C^S(\mathbf{x},\mathbf{x},a(\mathbf{x}),a(\mathbf{x})) = 1$ for any $\mathbf{x}$. Such a volume is (Liang and Marcotte 2016)

$$V(\mathbf{x},\mathbf{x}') = \begin{cases} \frac{\pi}{6}(\min\{a(\mathbf{x}),a(\mathbf{x}')\})^3 \\ \text{if } 0 < 2||\mathbf{x}-\mathbf{x}'|| < \max\{a(\mathbf{x})-a(\mathbf{x}'),a(\mathbf{x}')-a(\mathbf{x})\} \\ \frac{\pi\left(\frac{a(\mathbf{x})+a(\mathbf{x}')}{2} - ||\mathbf{x}-\mathbf{x}'||\right)^2\left(||\mathbf{x}-\mathbf{x}'||^2 + 2||\mathbf{x}-\mathbf{x}'||\frac{a(\mathbf{x})+a(\mathbf{x}')}{2} - 3\left(\frac{a(\mathbf{x})-a(\mathbf{x}')}{2}\right)^2\right)}{12||\mathbf{x}-\mathbf{x}'||} \\ \text{if } \max\{a(\mathbf{x})-a(\mathbf{x}'),a(\mathbf{x}')-a(\mathbf{x})\} < 2||\mathbf{x}-\mathbf{x}'|| < a(\mathbf{x})+a(\mathbf{x}') \\ 0 \quad \text{otherwise.} \end{cases} \quad (31)$$

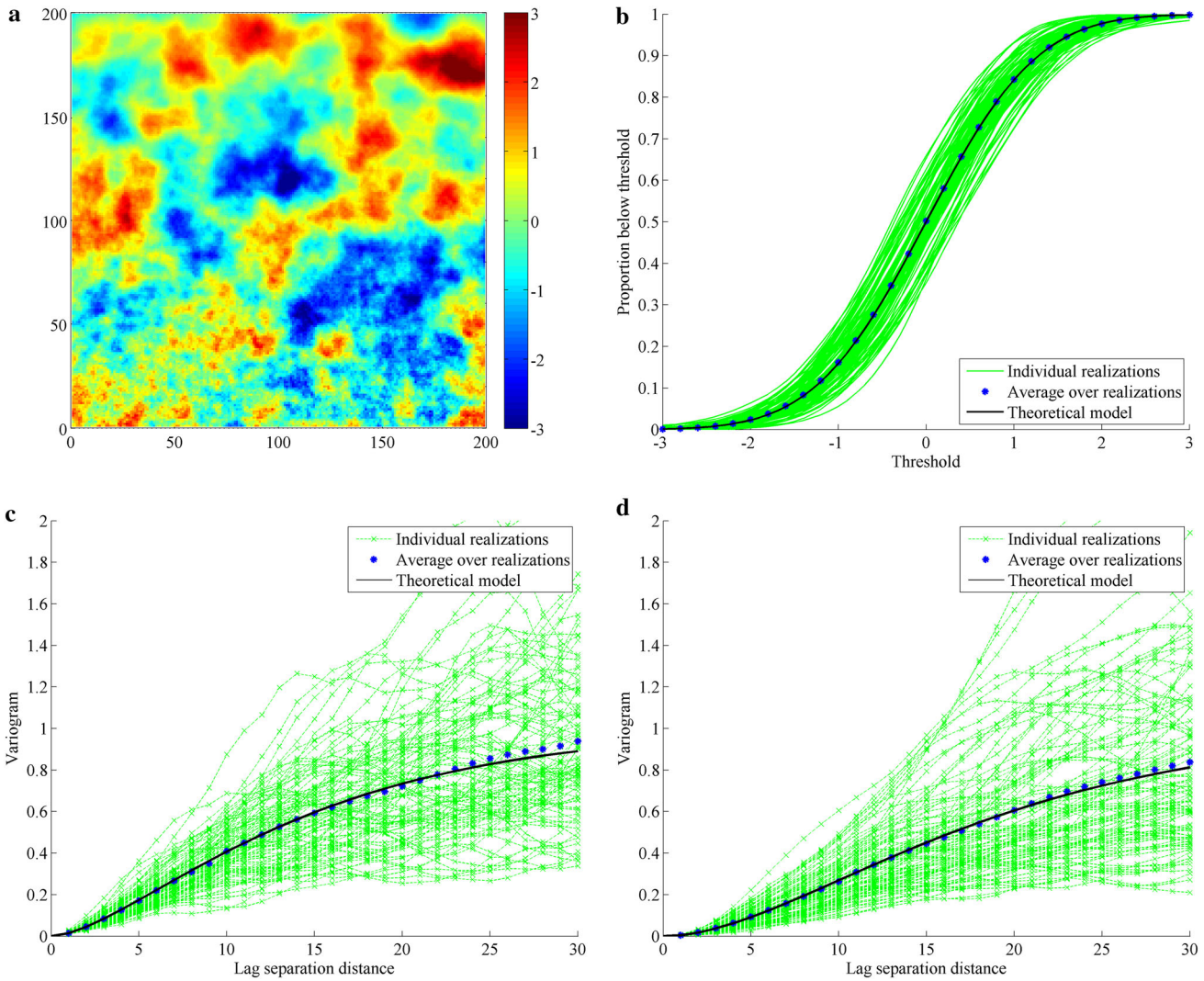

Fig. 3 **a** Realization of a random field with non-stationary Matérn covariance with varying shape parameter, **b** cumulative distribution functions of 100 realizations, and **c**, **d** local variograms of 100 realizations

Accordingly, the covariance is

$$C^S(\mathbf{x}, \mathbf{x}', a(\mathbf{x}), a(\mathbf{x}')) = \frac{V(\mathbf{x}, \mathbf{x}')}{\sqrt{V(\mathbf{x}, \mathbf{x})\, V(\mathbf{x}', \mathbf{x}')}}. \quad (32)$$

Chilès and Delfiner (2012) and Liang and Marcotte (2016) propose dilution and moving average algorithms to simulate a random field with such a non-stationary covariance. A realization obtained with the proposed spectral method on a 201 × 201 regular grid (with the same implementation parameters as previously: $L = 5000$ and g is the spectral density of a Matérn covariance with scale factor 3 and shape parameter 0.3) is mapped in Fig. 5a, where the range varies linearly with the ordinate axis, from $a(x, 0) = 5$ to $a(x, 200) = 30$. As for the previous experiments, the experimental cumulative distribution functions of one hundred realizations fluctuate without bias around the theoretical model (Fig. 5b), and the same happens with their experimental variograms calculated between the grid nodes with coordinates $(x, 100)$ and $(x, 100 - h)$ [resp. $(x, 200)$ and $(x, 200 - h)$], where x goes from 0 to 200, for lag separation distances h varying between 0 and 30 (Fig. 5c, d), indicating an accurate reproduction of the desired spatial correlation structure.

3 Multivariate simulation

3.1 Methodology

One can extend the previous spectral algorithm to the simulation of a non-stationary vector random field with P cross-correlated components, by considering a $P \times P$ matrix of spectral densities $\mathbf{f_x}$ (a Hermitian, positive semi-

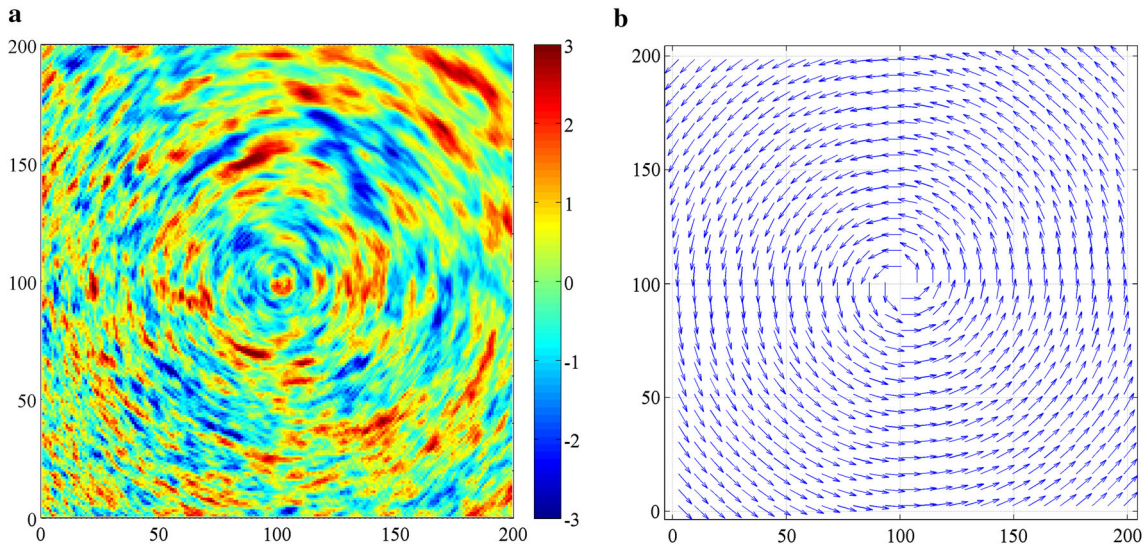

Fig. 4 **a** Realization of a random field with non-stationary Matérn covariance with varying scale factors, anisotropy directions and shape parameter. **b** Vectors indicating the local anisotropy azimuth for the direction with the largest scale factor

definite matrix) instead of a scalar spectral density $f_{\mathbf{x}}$. Specifically, let us define a non-stationary vector random field as follows:

$$\forall \mathbf{x} \in \mathbb{R}^d, \mathbf{Y}(\mathbf{x}) = \sum_{p=1}^{P} \alpha_{\mathbf{x},p}(\mathbf{u}_p) \cos\big(\langle \mathbf{u}_p | \mathbf{x} \rangle + \phi_p\big), \tag{33}$$

where $\{\mathbf{u}_p : p = 1, \ldots, P\}$ are mutually independent random vectors with density g, $\{\phi_p : p = 1, \ldots, P\}$ are mutually independent uniform random variables in $[0, 2\pi]$, independent of $\{\mathbf{u}_p : p = 1, \ldots, P\}$, and $\{\alpha_{\mathbf{x},p} : p = 1, \ldots, P\}$ are vector functions with P real-valued components that depend on the target location $\mathbf{x}$.

It is straightforward to show that the vector random field $\mathbf{Y}$ so defined has a zero mean. The covariance between $\mathbf{Y}(\mathbf{x})$ and $\mathbf{Y}(\mathbf{x}')$ is

$$\begin{aligned}
\mathbf{C}(\mathbf{x}, \mathbf{x}') &:= E\big\{\mathbf{Y}(\mathbf{x})\mathbf{Y}(\mathbf{x}')^T\big\} \\
&= \sum_{p=1}^{P}\sum_{q=1}^{P} E\Big\{\alpha_{\mathbf{x},p}(\mathbf{u}_p)\alpha_{\mathbf{x}',q}^T(\mathbf{u}_q)\cos\big(\langle \mathbf{u}_p|\mathbf{x}\rangle + \phi_p\big) \\
&\quad \times \cos\big(\langle \mathbf{u}_q|\mathbf{x}'\rangle + \phi_q\big)\Big\} \\
&= \sum_{p=1}^{P}\sum_{q=1}^{P} E\Big\{\alpha_{\mathbf{x},p}(\mathbf{u}_p)\alpha_{\mathbf{x}',q}^T(\mathbf{u}_q) \\
&\quad \times \frac{\cos\big(\langle \mathbf{u}_p|\mathbf{x}\rangle - \langle \mathbf{u}_q|\mathbf{x}'\rangle + \phi_p - \phi_q\big) + \cos\big(\langle \mathbf{u}_p|\mathbf{x}\rangle + \langle \mathbf{u}_q|\mathbf{x}'\rangle + \phi_p + \phi_q\big)}{2}\Big\}.
\end{aligned} \tag{34}$$

Since $\{\phi_p : p = 1, \ldots, P\}$ are mutually independent and uniformly distributed in $[0, 2\pi]$, the cosine terms in the previous expression have a zero expectation, except for $p = q$. Equation (34) therefore simplifies into:

$$\begin{aligned}
\mathbf{C}(\mathbf{x}, \mathbf{x}') &= E\left\{\frac{1}{2}\sum_{p=1}^{P} \alpha_{\mathbf{x},p}(\mathbf{u}_p)\alpha_{\mathbf{x}',p}^T(\mathbf{u}_p)\cos\big(\langle \mathbf{u}_p|\mathbf{x}-\mathbf{x}'\rangle\big)\right\} \\
&= \frac{1}{2}\int_{\mathbb{R}^d} \mathbf{A}_{\mathbf{x}}(\mathbf{u})\,\mathbf{A}_{\mathbf{x}'}^T(\mathbf{u})\cos(\langle \mathbf{u}|\mathbf{x}-\mathbf{x}'\rangle) g(\mathbf{u}) d\mathbf{u} \\
&= \mathrm{F}\left\{\frac{\mathbf{A}_{\mathbf{x}}\mathbf{A}_{\mathbf{x}'}^T}{2} g\right\}(\mathbf{x}-\mathbf{x}'),
\end{aligned} \tag{35}$$

where $\mathbf{A}_{\mathbf{x}}(\mathbf{u})$ and $\mathbf{A}_{\mathbf{x}'}(\mathbf{u})$ are the $P \times P$ matrices whose p-th columns are $\alpha_{\mathbf{x},p}(\mathbf{u})$ and $\alpha_{\mathbf{x}',p}(\mathbf{u})$, respectively.

To obtain a vector random field with multivariate Gaussian finite-dimensional distributions, again it is necessary to sum numerous independent components defined as in Eq. (33):

$$\forall \mathbf{x} \in \mathbb{R}^d, \mathbf{Y}(\mathbf{x}) = \frac{1}{\sqrt{L}}\sum_{l=1}^{L}\sum_{p=1}^{P} \alpha_{\mathbf{x},p}(\mathbf{u}_{l,p})\cos\big(\langle \mathbf{u}_{l,p}|\mathbf{x}\rangle + \phi_{l,p}\big), \tag{36}$$

where L is a large integer, $\{\mathbf{u}_{l,p} : l = 1, \ldots, L; p = 1, \ldots, P\}$ are mutually independent random vectors with density g, and $\{\phi_{l,p} : l = 1, \ldots, L; p = 1, \ldots, P\}$ are mutually independent random variables uniformly distributed in $[0, 2\pi]$, independent of $\{\mathbf{u}_{l,p} : l = 1, \ldots, L; p = 1, \ldots, P\}$.

3.2 First example: vector random field with non-stationary Gaussian covariance

Let us simulate a vector random field $\mathbf{Y}$ with $P = 2$ components by using the following 2×2 matrix $\mathbf{A}_{\mathbf{x}}(\mathbf{u})$:

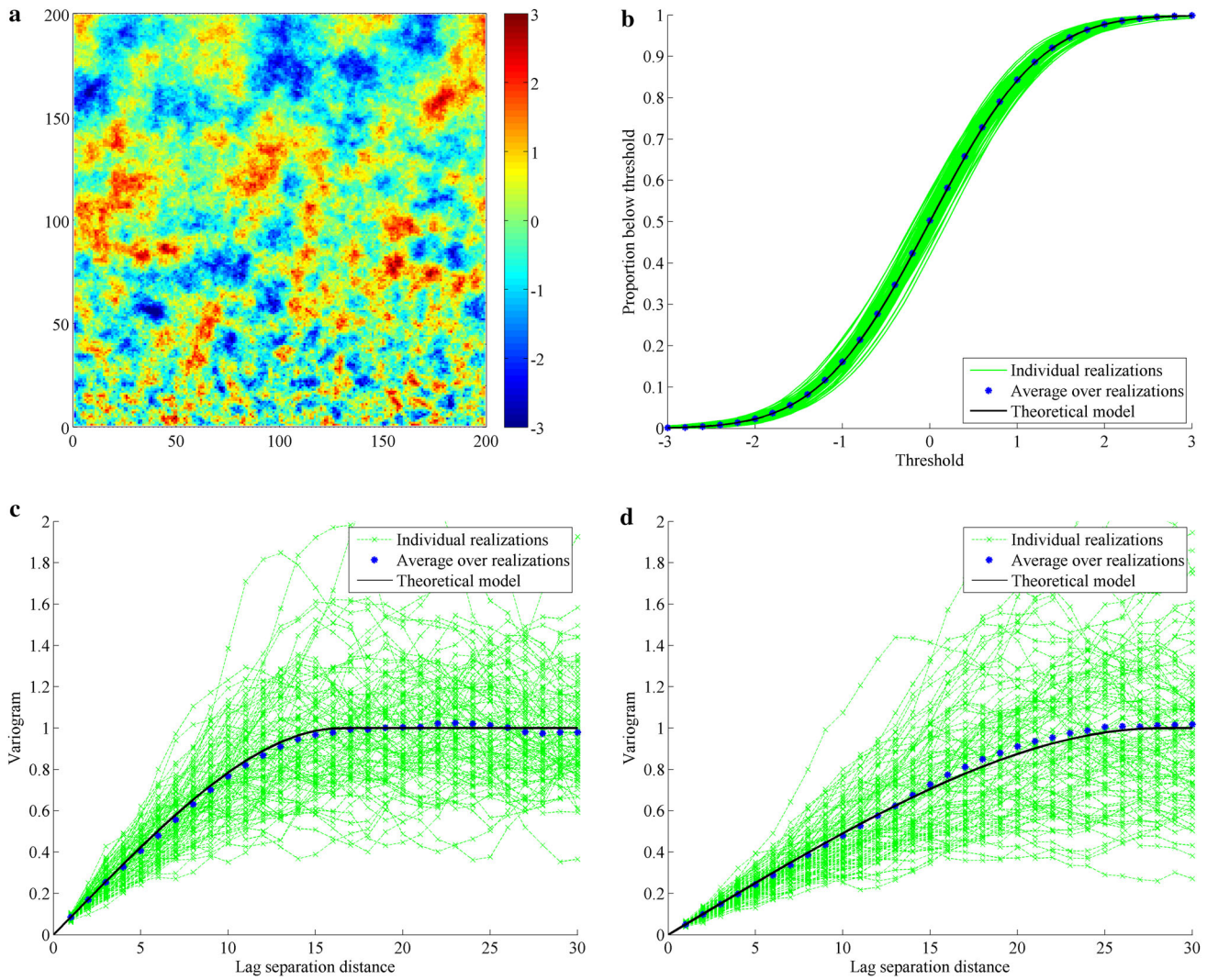

Fig. 5 **a** Realization of a random field with non-stationary spherical covariance with varying range, **b** cumulative distribution functions of 100 realizations, and **c**, **d** local variograms of 100 realizations

$$\forall \mathbf{x} \in \mathbb{R}^d, \mathbf{A}_{\mathbf{x}}(\mathbf{u}) = \sqrt{\frac{2}{g(\mathbf{u})}} \begin{pmatrix} \sqrt{f^G_{\Sigma^{11}_{\mathbf{x}}}(\mathbf{u})} & 0 \\ \rho\sqrt{f^G_{\Sigma^{22}_{\mathbf{x}}}(\mathbf{u})} & \sqrt{1-\rho^2}\sqrt{f^G_{\Sigma^{22}_{\mathbf{x}}}(\mathbf{u})} \end{pmatrix}, \tag{37}$$

where $\Sigma^{11}_{\mathbf{x}}$ and $\Sigma^{22}_{\mathbf{x}}$ are symmetric positive semi-definite matrices, f^G_{Σ} is the spectral density of the Gaussian covariance with anisotropy matrix Σ (Eqs. 12 and 14), g is the probability density function of $\mathbf{u}$ and $\rho \in [-1, 1]$.

According to Eq. (35), the covariance between $\mathbf{Y}(\mathbf{x})$ and $\mathbf{Y}(\mathbf{x}')$ is:

$$\mathbf{C}^G\left(\mathbf{x}, \mathbf{x}', \Sigma^{11}_{\mathbf{x}}, \Sigma^{11}_{\mathbf{x}'}, \Sigma^{22}_{\mathbf{x}}, \Sigma^{22}_{\mathbf{x}'}, \rho\right) = \mathrm{F}\begin{pmatrix} \sqrt{f^G_{\Sigma^{11}_{\mathbf{x}}}(\mathbf{u}) f^G_{\Sigma^{11}_{\mathbf{x}'}}(\mathbf{u})} & \rho\sqrt{f^G_{\Sigma^{11}_{\mathbf{x}}}(\mathbf{u}) f^G_{\Sigma^{22}_{\mathbf{x}'}}(\mathbf{u})} \\ \rho\sqrt{f^G_{\Sigma^{22}_{\mathbf{x}}}(\mathbf{u}) f^G_{\Sigma^{11}_{\mathbf{x}'}}(\mathbf{u})} & \sqrt{f^G_{\Sigma^{22}_{\mathbf{x}}}(\mathbf{u}) f^G_{\Sigma^{22}_{\mathbf{x}'}}(\mathbf{u})} \end{pmatrix}(\mathbf{x} - \mathbf{x}'). \tag{38}$$

One finds (Eq. 15):

$$\mathbf{C}^G(\mathbf{x}, \mathbf{x}', \Sigma^{11}_{\mathbf{x}}, \Sigma^{11}_{\mathbf{x}'}, \Sigma^{22}_{\mathbf{x}}, \Sigma^{22}_{\mathbf{x}'}, \rho) = \begin{pmatrix} C^G(\mathbf{x}, \mathbf{x}', \Sigma^{11}_{\mathbf{x}}, \Sigma^{11}_{\mathbf{x}'}) & \rho C^G(\mathbf{x}, \mathbf{x}', \Sigma^{11}_{\mathbf{x}}, \Sigma^{22}_{\mathbf{x}'}) \\ \rho C^G(\mathbf{x}, \mathbf{x}', \Sigma^{22}_{\mathbf{x}}, \Sigma^{11}_{\mathbf{x}'}) & C^G(\mathbf{x}, \mathbf{x}', \Sigma^{22}_{\mathbf{x}}, \Sigma^{22}_{\mathbf{x}'}) \end{pmatrix}. \tag{39}$$

All the direct and cross covariances are Gaussian, with anisotropy matrices that depend on both locations $\mathbf{x}$ and $\mathbf{x}'$. The scalar ρ is nothing else than the correlation coefficient between the two components of $\mathbf{Y}$ at the same location $\mathbf{x}$. Note that there is no specific restriction on the anisotropy matrices, other than being positive semi-definite, or on the correlation coefficient, other than belonging to the interval $[-1, 1]$.

For instance, consider a bivariate random field on a regular two dimensional grid with 201 × 201 nodes, where the first component has an anisotropic Gaussian covariance

with the largest (resp. smallest) practical range that linearly varies from 25 (resp. 10) for $x = 0$ to 75 (resp. 30) for $x = 200$, while the second component has an anisotropic Gaussian covariance with the largest (resp. smallest) practical range that linearly varies from 50 (resp. 10) for $x = 0$ to 150 (resp. 30) for $x = 200$, so that the anisotropy ratio remains constant in space for each component. Also, consider spatially varying azimuths for the directions with largest practical ranges, as indicated in Fig. 4b, and a collocated correlation coefficient between both components equal to 0.7. A realization of such a bivariate random field, constructed by using $L = 5000$ lines and the spectral density of a Matérn covariance with scale factor 3 and shape parameter 0.3 for g, is mapped in Fig. 6.

3.3 Second example: vector random field with non-stationary Matérn covariance

To end up, let us modify the previous construction as follows:

$$\forall \mathbf{x} \in \mathbb{R}^d, \mathbf{A}_{\mathbf{x},l}(\mathbf{u}) = \sqrt{\frac{2}{g(\mathbf{u})}} \begin{pmatrix} \sqrt{f^M_{\Sigma^{11}_{\mathbf{x}},\mu_{11}(\mathbf{x}),a_l}(\mathbf{u})} & 0 \\ \rho\sqrt{f^M_{\Sigma^{22}_{\mathbf{x}},\mu_{22}(\mathbf{x}),a_l}(\mathbf{u})} & \sqrt{1-\rho^2}\sqrt{f^M_{\Sigma^{22}_{\mathbf{x}},\mu_{22}(\mathbf{x}),a_l}(\mathbf{u})} \end{pmatrix}, \tag{40}$$

where $l = 1, \ldots, L$ is the line index, a_l is a realization of an exponential variable, $\mu_{11}(\mathbf{x})$ and $\mu_{22}(\mathbf{x})$ are positive scalars that depend on $\mathbf{x}$, and $f^M_{\Sigma,\mu,a}(\mathbf{u}) = \frac{a^{\mu-1}}{\Gamma(\mu)} f^G_{4a\Sigma}(\mathbf{u})$ (Eq. 26). The covariance between $\mathbf{Y}(\mathbf{x})$ and $\mathbf{Y}(\mathbf{x}')$ becomes:

The direct and cross covariance functions turn out to be Matérn covariances, with spatially varying anisotropy matrices and shape parameters. As an illustration, consider a regular grid with 201 × 201 nodes and define a bivariate covariance model, where the first direct covariance is a stationary and isotropic Matérn covariance with scale parameter 10 and constant shape parameter $\mu_{11} = 0.5$, the second direct covariance is an isotropic Matérn covariance with scale parameter 10 and shape parameter $\mu_{22}(x, y)$ that varies linearly with y, such that $\mu_{22}(x, 0) = 0.5$ and $\mu_{22}(x, 200) = 1.5$, and the collocated correlation coefficient ρ is 0.6. Spectral simulation is performed with $L = 5000$ lines and with the spectral density of an isotropic Matérn covariance with scale factor 3 and shape parameter 0.3 for g. Figure 7 shows the map of one realization, in which the first component (Fig. 7a) looks homogeneous in space with rough spatial variations, while the second component (Fig. 7b) looks heterogeneous, with progressively smoother spatial variations when getting closer to the top of the map (higher shape parameter). Figure 8a, c, e (resp. Fig. 8b, d, f) compare the experimental direct and cross variograms of one hundred realizations, calculated between the grid nodes with coordinates $(x, 100)$ and $(x, 100 - h)$ [resp. $(x, 200)$ and $(x, 200 - h)$], where x goes from 0 to 200, for lag separation distances h varying between 0 and 30, with the corresponding theoretical variograms. In both cases, the average of the experimental variograms matches quite well the corresponding theoretical model, indicating an accurate reproduction of the coregionalization model.

$$\mathbf{C}^M(\mathbf{x},\mathbf{x}',\Sigma^{11}_{\mathbf{x}},\Sigma^{11}_{\mathbf{x}'},\Sigma^{22}_{\mathbf{x}},\Sigma^{22}_{\mathbf{x}'},\mu_{11}(\mathbf{x}),\mu_{11}(\mathbf{x}'),\mu_{22}(\mathbf{x}),\mu_{22}(\mathbf{x}'),\rho) = E\left\{ \mathrm{F} \begin{pmatrix} \sqrt{f^M_{\Sigma^{11}_{\mathbf{x}},\mu_{11}(\mathbf{x}),a_l}(\mathbf{u}) f^M_{\Sigma^{11}_{\mathbf{x}'},\mu_{11}(\mathbf{x}'),a_l}(\mathbf{u})} & \rho\sqrt{f^M_{\Sigma^{11}_{\mathbf{x}},\mu_{11}(\mathbf{x}),a_l}(\mathbf{u}) f^M_{\Sigma^{22}_{\mathbf{x}'},\mu_{22}(\mathbf{x}'),a_l}(\mathbf{u})} \\ \rho\sqrt{f^M_{\Sigma^{22}_{\mathbf{x}},\mu_{22}(\mathbf{x}),a_l}(\mathbf{u}) f^M_{\Sigma^{11}_{\mathbf{x}'},\mu_{11}(\mathbf{x}'),a_l}(\mathbf{u})} & \sqrt{f^M_{\Sigma^{22}_{\mathbf{x}},\mu_{22}(\mathbf{x}),a_l}(\mathbf{u}) f^M_{\Sigma^{22}_{\mathbf{x}'},\mu_{22}(\mathbf{x}'),a_l}(\mathbf{u})} \end{pmatrix} \right\}(\mathbf{x}-\mathbf{x}'), \tag{41}$$

where the expected value is taken with respect to the exponential variable a_l. It comes (Eq. 27):

$$\mathbf{C}^M(\mathbf{x},\mathbf{x}',\Sigma^{11}_{\mathbf{x}},\Sigma^{11}_{\mathbf{x}'},\Sigma^{22}_{\mathbf{x}},\Sigma^{22}_{\mathbf{x}'},\mu_{11}(\mathbf{x}),\mu_{11}(\mathbf{x}'),\mu_{22}(\mathbf{x}),\mu_{22}(\mathbf{x}'),\rho) = \begin{pmatrix} C^M(\mathbf{x},\mathbf{x}',\Sigma^{11}_{\mathbf{x}},\Sigma^{11}_{\mathbf{x}'},\mu_{11}(\mathbf{x}),\mu_{11}(\mathbf{x}')) & \rho C^M(\mathbf{x},\mathbf{x}',\Sigma^{11}_{\mathbf{x}},\Sigma^{22}_{\mathbf{x}'},\mu_{11}(\mathbf{x}),\mu_{22}(\mathbf{x}')) \\ \rho C^M(\mathbf{x},\mathbf{x}',\Sigma^{22}_{\mathbf{x}},\Sigma^{11}_{\mathbf{x}'},\mu_{22}(\mathbf{x}),\mu_{11}(\mathbf{x}')) & C^M(\mathbf{x},\mathbf{x}',\Sigma^{22}_{\mathbf{x}},\Sigma^{22}_{\mathbf{x}'},\mu_{22}(\mathbf{x}),\mu_{22}(\mathbf{x}')) \end{pmatrix}. \tag{42}$$

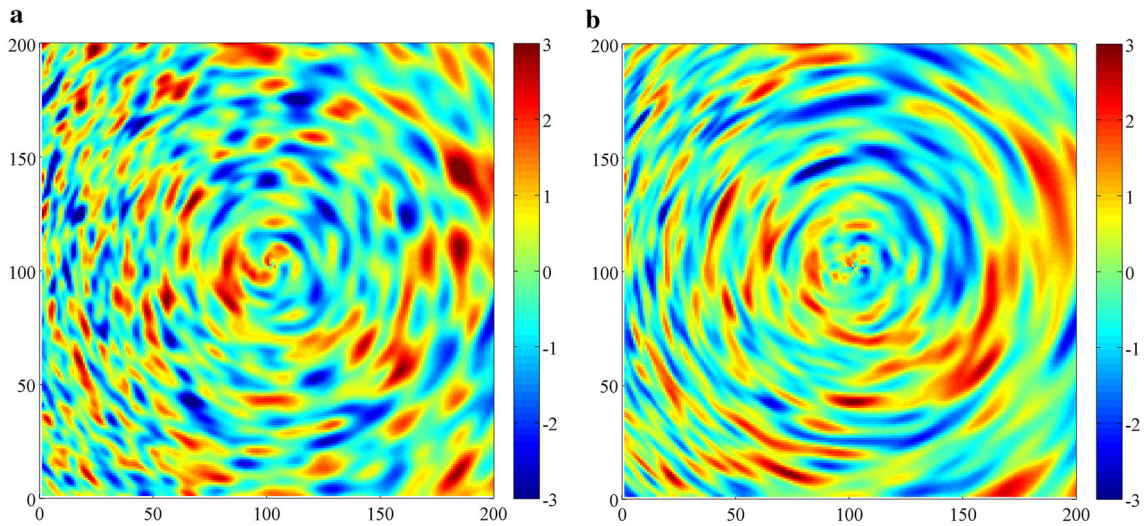

Fig. 6 Realization of a vector random field with non-stationary Gaussian direct and cross covariances. **a** first component, **b** second component

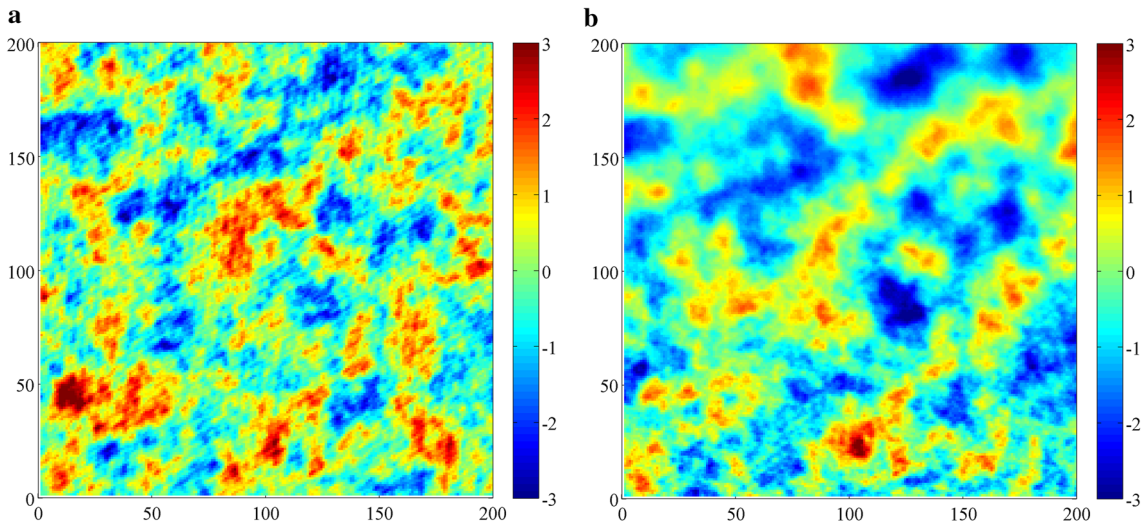

Fig. 7 Realization of a vector random field with non-stationary Matérn direct and cross covariances. **a** first component, **b** second component

4 Discussion and conclusions

The algorithm presented in this paper is an extension to the non-stationary framework of the spectral-turning bands algorithm developed by Emery et al. (2016) and stands out for its versatility, accuracy and low computational requirements. Indeed:

1. Because one has a functional expression of the simulated field as a weighted sum of cosine waves (Eqs. 9 and 36), realizations of this field can be constructed at as many locations as desired, irrespective of whether these locations are evenly spaced or not.
2. Many non-stationary covariance models can be reproduced, as illustrated in the examples throughout this paper. In particular, the models developed by Paciorek and Schervish (2006) can be viewed as scale mixtures of non-stationary Gaussian covariances and simulated in a way similar to the one indicated in Sects. 2.3.3 and 2.3.4. The extension to multivariate models is also straightforward, as shown in Sect. 3.
3. Simulation is accurate, in the sense that the desired spatial correlation structure (non-stationary covariance function) is reproduced without any bias. The only approximation lies in the use of a finite set of turning lines, which makes the finite-dimensional distributions of the simulated random field not perfectly multivariate Gaussian.
4. The process time is proportional to the number L of lines and to the number of target locations and can be improved by resorting to parallel computing. Storage requirements are also minimal, insofar as the field can

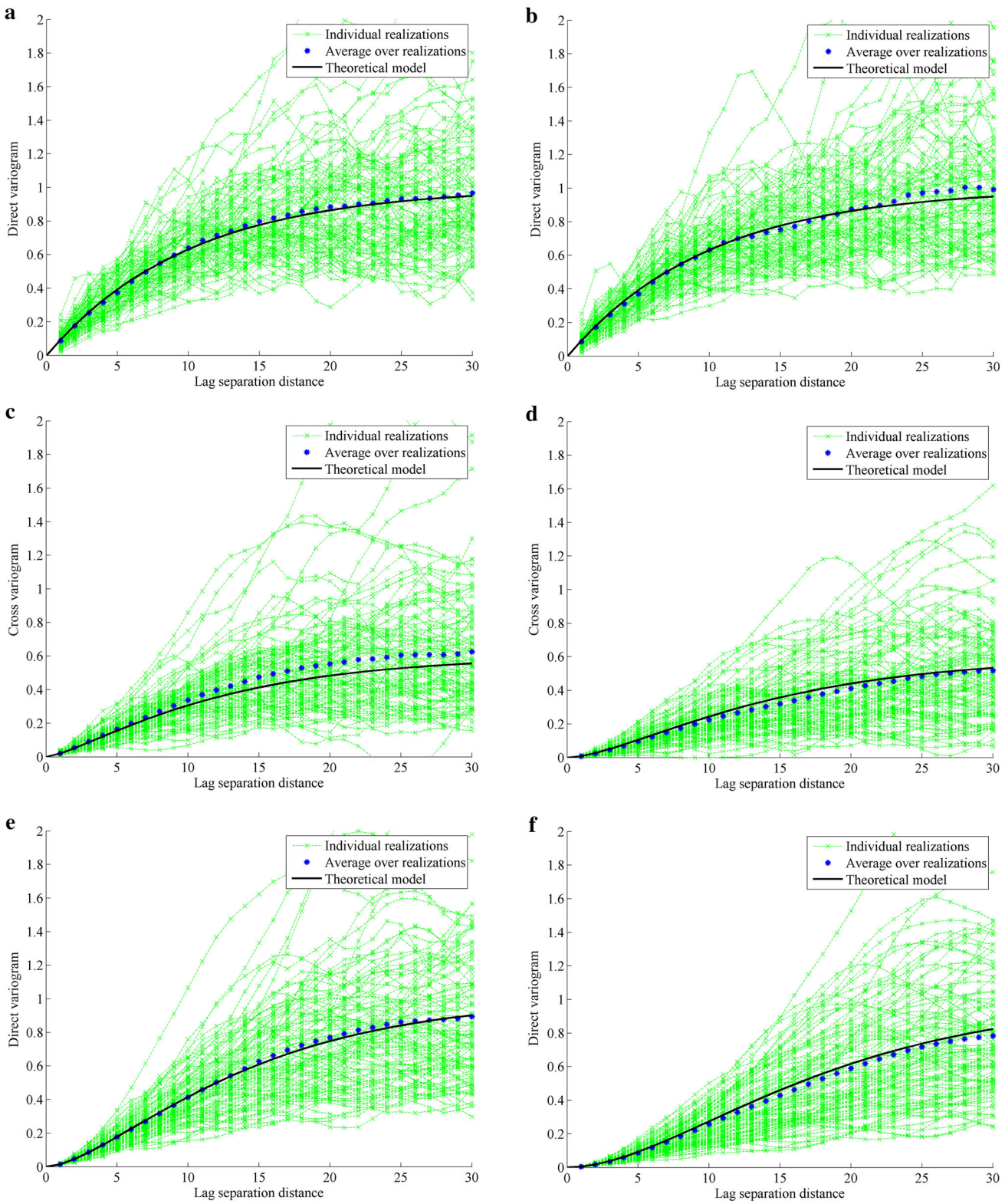

Fig. 8 Local variograms of 100 realizations of vector random field with non-stationary Matérn covariances: **a**, **b** direct variograms for first component, **c**, **d** cross variograms, and **e**, **f** direct variograms for second component

be simulated at any subset of target locations and the results stored, without the need for knowing the values at the other locations.

The setting of the algorithm turns out to be particularly simple and its applicability has been illustrated through varied numerical examples, where scalar and vector random fields with non-stationary Gaussian, exponential, Matérn or compactly-supported covariance models have been simulated. As a suggestion for future researches, one may focus on analyzing the convergence of the simulated fields to Gaussian random fields, as a function of the number L of lines and the chosen density g for the frequency vectors. Indeed, these two parameters (L and g) can have an impact on the spread of statistical fluctuations, as well as on the spatial behavior of the simulated field that can be qualitatively assessed by mapping the realizations. In our experience, it is more convenient to choose a density g that favors the occurrence of large frequencies (for instance, the density of a Matérn covariance with small shape parameter, such as the one taken in the presented numerical experiments), thus a better reproduction of the short-scale behavior of the simulated field for a given number L of lines.

Acknowledgements The authors are grateful to two anonymous reviewers for their constructive comments and acknowledge the support of the Chilean Commission for Scientific and Technological Research, through Projects CONICYT PIA Anillo ACT1407 and CONICYT/FONDECYT/POSTDOCTORADO/N°3140568.

References

Arroyo D, Emery X (2017) Spectral simulation of vector random fields with stationary Gaussian increments in d-dimensional Euclidean spaces. Stoch Environ Res Risk Assess. doi:10.1007/s00477-016-1225-7

Bochner S (1933) Monotone funktionen, Stieljessche integrale und harmonische analyse. Math Ann 108:378–410

Boisvert JB, Deutsch CV (2011) Programs for kriging and sequential Gaussian simulation with locally varying anisotropy using non-Euclidean distances. Comput Geosci 37(4):495–510

Chilès JP, Delfiner P (2012) Geostatistics: modeling spatial uncertainty, 2nd edn. Wiley, New York

Costa JF (2009) Interpolating datasets with trends: a modified median polish approach. Comput Geosci 35(11):2222–2230

Damian D, Sampson PD, Guttorp P (2000) Bayesian estimation of semi-parametric non-stationary spatial covariance structure. Environmetrics 12(2):161–178

Deutsch CV, Journel AG (1998) GSLIB: geostatistical software library and user's guide. Oxford University Press, New York

Emery X, Lantuéjoul C (2006) TBSIM: a computer program for conditional simulation of three-dimensional Gaussian random fields via the turning bands method. Comput Geosci 32(10):1615–1628

Emery X, Lantuéjoul C (2008) A spectral approach to simulating intrinsic random fields with power and spline generalized covariances. Comput Geosci 12(1):121–132

Emery X, Arroyo D, Porcu E (2016) An improved spectral turning-bands algorithm for simulating stationary vector Gaussian random fields. Stoch Environ Res Risk Assess 30(7):1863–1873

Fouedjio F, Séguret S (2016) Predictive geological mapping using closed-form non-stationary covariance functions with locally varying anisotropy: case study at El Teniente Mine (Chile). Nat Resour Res 25(4):431–443

Fouedjio F, Desassis N, Rivoirard J (2016) A generalized convolution model and estimation for non-stationary random functions. Spat Stat 16:35–52

Fuentes M (2002) Interpolation of nonstationary air pollution processes: a spatial spectral approach. Stat Model 2(4):281–298

Goovaerts P (1997) Geostatistics for natural resources evaluation. Oxford University Press, New York

Guttorp P, Sampson PD (1994) Methods for estimating heterogeneous spatial covariance functions with environmental applications. In: Patil GP, Rao CR (eds) Handbook of statistics XII: environmental statistics. Elsevier, New York, pp 663–690

Haas TC (1990) Kriging and automated variograms modeling within a moving window. Atmos Environ Part A Gen Top 24(7):1759–1769

Harris P, Charlton M, Fotheringham AS (2010) Moving window kriging with geographically weighted variograms. Stoch Environ Res Risk Assess 24(8):1193–1209

Higdon D (2002) Space and space-time modeling using process convolutions. In: Anderson CW, Barnett V, Chatwin PC, El-Shaarawi AH (eds) Quantitative methods for current environmental issues. Springer, London, pp 37–56

Higdon D, Swall J, Kern J (1999) Non-stationary spatial modeling. In: Bernardo JM, Berger JO, Dawid AP, Smith AFM (eds) Bayesian statistics 6—proceedings of the sixth Valencia international meeting. Oxford University Press, New York, pp 761–768

Journel AG (1986) Geostatistics: models and tools for the earth sciences. Math Geol 18(1):119–140

Journel AG, Huijbregts CJ (1978) Mining geostatistics. Academic Press, London

Lantuéjoul C (2002) Geostatistical simulation: models and algorithms. Springer, Berlin

Liang M, Marcotte D (2016) A class of non-stationary covariance functions with compact support. Stoch Environ Res Risk Assess 30(3):973–987

Machuca-Mory DF, Deutsch CV (2013) Non-stationary geostatistical modeling based on distance weighted statistics and distributions. Math Geosci 45(1):31–48

Marcotte D (2015) TASC3D: a program to test the admissibility in 3D of non-linear models of coregionalization. Comput Geosci 83:168–175

Matheron G (1971) The theory of regionalized variables and its applications. Ecole des Mines de Paris, Fontainebleau

Matheron G (1973) The intrinsic random functions and their applications. Adv Appl Probab 5:439–468

Matheron G (1989) Estimating and choosing. Springer, Berlin

Monestiez P, Switzer P (1991) Semiparametric estimation of nonstationary spatial covariance models by metric multidimensional scaling. Technical report, Stanford University, USA

Nychka D, Wikle C, Royle A (2002) Multiresolution models for nonstationary spatial covariance functions. Stat Model 2(4):315–331

Paciorek CJ, Schervish MJ (2006) Spatial modelling using a new class of nonstationary covariance functions. Environmetrics 17(5):483–506

Pintore A, Holmes CC (2005) A dimension-reduction approach for spectral tempering using empirical orthogonal functions. In: Leuangthong O, Deutsch CV (eds) Geostatistics Banff 2004. Springer, Dordrecht, pp 1007–1015

Sampson PD, Guttorp PT (1992) Nonparametric estimation of nonstationary spatial covariance structure. J Am Stat Assoc 87(417):108–119

Sampson PD, Damian D, Guttorp P (2001) Advances in modeling and inference for environmental processes with nonstationary spatial covariance. In: Monestiez P, Allard D, Froidevaux R (eds) Proceedings of the third European conference on geostatistics for environmental applications geoENV III. Springer, Dordrecht, pp 17–32

Schlather M (2010) Some covariance models based on normal scale mixtures. Bernoulli 16(3):780–797

Shinozuka M (1971) Simulation of multivariate and multidimensional random processes. J Acoust Soc Am 49(1B):357–367

Shinozuka M, Jan CM (1972) Digital simulation of random processes and its applications. J Sound Vib 25(1):111–128

Smith RL (1996) Estimating nonstationary spatial correlations. University of North Carolina, Chapel Hill

Stein M (2005) Non-stationary spatial covariance functions. Technical report, University of Chicago

Stephenson J, Holmes C, Gallagher K, Pintore A (2005) A statistical technique for modeling non-stationary spatial processes. In: Leuangthong O, Deutsch CV (eds) Geostatistics Banff 2004. Springer, Dordrecht, pp 125–134

Zhu Z, Wu Y (2010) Estimation and prediction of a class of convolution-based spatial nonstationary models for large spatial data. J Comput Graph Stat 19(1):74–95